Tutor/s

Dr. Xavier Vendrell Villafruela
Departament de Química Inorgànica i Orgànica, secció Química Inorgànica

Dr. Guilhem Dezanneau
Laboratory of Structures, Properties and Modelling of Solids, Centrale Supélec

Grau de Química

Treball Final de Grau

Deposition of $BaCo_{0.4}Fe_{0.4}Zr_{0.2}O_{3-\delta}$ material thin films through chemical solution via Spin-Coating.

Deposició de pel·lícules primes del material $BaCo_{0.4}Fe_{0.4}Zr_{0.2}O_{3-\delta}$ a través de solució química via Spin Coating.

Judith Gutiérrez Arce

Gener 2024

Universitat de Barcelona

B:KC Barcelona Knowledge Campus
Campus d'Excel·lència Internacional

Primero agradecer a mis tutores, al Dr. Xavier Vendrell y al Dr. Guilhem Dezanneau, y a la Dra. Lourdes Mestres por la oportunidad de haber podido hacer este trabajo en colaboración con todos ellos, aprendiendo mucho cada día.

Gracias a mis padres, a mi familia y a mis amigos por todo el apoyo y cariño constate día a día, aún en la distancia. Y finalmente, gracias a todas las personas de SPMS por haberme acogido de una manera tan especial durante estos meses.

REPORT

IDENTIFICATION AND REFLECTION ON THE SUSTAINABLE DEVELOPMENT GOALS (SDG)

This research project aims to further develop a depositing technique for a new material for protonic solid oxide fuel cells and thus aligns with several United Nations Sustainable Development Goals (SDGs) due to its potential impact on renewable energy and environmental sustainability. Additionally, the project's success could attract investment, collaboration, and global knowledge, accelerating the adoption of sustainable technologies and promoting a greener future.

SDG 7: Affordable and Clean Energy

Protonic solid oxide fuel cells are a type of fuel cell that uses a proton-conducting electrolyte instead of a traditional oxygen-ion-conducting electrolyte. This design offers several advantages, including higher energy conversion efficiency and the ability to operate at lower temperatures. In agreement with SDG 7, this research project aims to contribute to the advancement of clean and sustainable energy technology by further developing a novel material for protonic solid oxide fuel cells, potentially improving energy conversion efficiency, and reducing reliance on fossil fuels.

SDG 9: Industry, Innovation, and Infrastructure

For SDG 9, the research project contributes to the goals of industry, innovation, and infrastructure by developing innovative techniques for material deposition through chemical solutions via spin-coating. The project's goal is to integrate the developed materials into existing industrial infrastructure, leading to large-scale production of advanced energy materials.

However, negative outcomes could relate to technological challenges, scalability issues, or environmental impacts associated with the production process.

SDG 12: Responsible Consumption and Production

The project aims to promote responsible consumption and production by developing a material for clean energy, contributing to sustainable resource use. More specifically, the spin coating technique improves the characteristics and properties of the material while minimizing the number of primary materials and energy needed for its preparation and functioning. Positive outcomes include optimizing material usage and reducing waste, while negative ones involve challenges in sourcing raw materials responsibly and managing waste.

SDG 13: Climate Action

The research project aims to address climate change by developing a material for protonic solid oxide fuel cells, potentially reducing greenhouse gas emissions by reducing carbon dioxide emissions. The ultimate future objective involves widespread implementation of protonic solid oxide fuel cells, contributing significantly to global efforts to combat climate change and transition to a low-carbon economy.

In conclusion, the research project has the potential to significantly impact clean energy, materials science, and sustainable technology. It could lead to energy efficiency improvements and reduced environmental impact while also addressing challenges like scalability and societal adoption of new technologies. The continuity of the project will contribute to advancing clean energy solutions, fostering innovation, and achieving UN Sustainable Development Goals.

CONTENTS

1. SUMMARY

This final degree project studies the deposition of $BaCo_{0.4}Fe_{0.4}Zr_{0.2}O_{3-\delta}$ (BCFZO) thin films using a chemical solution-based spin-coating technique for potential use in solid oxide fuel cells (SOFCs). It emphasises the importance of precise stoichiometric measurements, pH control, and characterization techniques, describes and studies the compound and its properties using XRD, optical microscopy, and electrical measurements. These techniques are essential for understanding the structural and electrical characteristics of the BCFZO thin films. Furthermore, the study investigates the effect of various deposition parameters, such as viscosity and spin rate, offering knowledge for improving the spin-coating process. Through the optimization, particularly with PEI-assisted synthesis and lower-temperature thermal treatments (600ºC), the production of homogeneous films demonstrates satisfactory electrical properties. Further experimentation is recommended, including trying different PEI ratios and thermal treatments, exploring other polymerization chemicals, and optimising the XRD characterization technique. The study offers useful knowledge and sets an orientation for future advances in BCFZO thin film deposition.

Keywords: thin films, spin coating, deposition, XRD, microscopy, PEI.

2. RESUMEN

Este trabajo de final de grado investiga la deposición de capas finas de $BaCo_{0.4}Fe_{0.4}Zr_{0.2}O_{3-\delta}$ (BCFZO) mediante una técnica de "spin-coating" basada en una solución química para su posible uso en pilas de combustible. El estudio destaca la importancia de las mediciones estequiométricas precisas, el control del pH y las técnicas de caracterización. Gracias a estas, se describe y estudia el compuesto y sus propiedades mediante DRX, microscopía óptica y mediciones eléctricas. Estas técnicas son esenciales para comprender las características estructurales y eléctricas de las capas finas de BCFZO. Además, el estudio investiga el efecto de varios parámetros de deposición, como la viscosidad y la velocidad de centrifugado, ofreciendo conocimiento para mejorar el proceso de spin-coating. Mediante una optimización, en particular con la síntesis asistida por PEI y los tratamientos térmicos a baja temperatura (600ºC), la producción de películas homogéneas demuestra unas propiedades eléctricas satisfactorias. Se recomienda seguir experimentando, probando diferentes proporciones de PEI y tratamientos térmicos, explorando otros reactivos polimerizantes y optimizar los parámetros de la caracterización por DRX. El estudio ofrece una orientación para futuros avances en la deposición de capas finas de BCFZO.

Palabras clave: Capas finas, spin-coating, deposición, DRX, microscopía, PEI.

3. INTRODUCTION

In the search of advanced materials for energy conversion and storage applications, perovskite-type oxides have developed as promising candidates due to their electrochemical properties. Among these materials, the $BaCo_{0.4}Fe_{0.4}Zr_{0.2}O_{3-\delta}$ (BCFZO) compound has gained significant attention for its potential use in solid oxide fuel cells.

The controlled deposition of BCFZO thin films is fundamental to maximizing its beneficial properties and optimizing their performance in practical applications. In this study, the deposition of BCFZO material using a chemical solution-based spin-coating technique is presented. The spin coating technique offers precise control over film thickness and microstructure, making it a helpful method for the fabrication of thin-film electrolytes and electrodes in various electrochemical devices.

Characterization plays a central role in interpreting the structural and electrical properties of deposited materials, which is essential for optimising their performance. Therefore, two fundamental characterization techniques were used: X-ray diffraction (XRD), optical microscopy and, to provide insights into the BCFZO thin films. On one end, XRD analysis allowed to probe the crystallographic structure and phase purity of the deposited BCFZO films. But, on the other hand, visual prove on the films thought optical microscopy, ensured good homogeneity of the films. Furthermore, the investigation will also explore the influence of different deposition parameters on the film's homogeneity and crystallinity, offering a deeper understanding of the fabrication process.

In addition to structural characterization, 2-point and 4-point electrical measurements were made to assess the electrical conductivity, resistance, and overall electrochemical performance of the BCFZO thin films. These measurements are essential for evaluating the viability of using BCFZO in solid oxide fuel cells.

Through this study, the aim was to provide valuable insights into the deposition of BCFZO material via chemical solution-based spin-coating and to achieve an optimal and reproducible procedure of BCFZO thin film deposition.

4. THEORY PRINCIPLES

4.1 SOLID-STATE CHEMISTRY

Solid-state chemistry is a branch of chemistry that focuses on the study between the internal structure and properties of solids. On one side, their structure is determined by the internal characterization techniques which can give information, such as composition, oxidation states, coordination requirements, and bonding preferences. On the other side, key information about the solid's characteristics, including their electrical, magnetic, thermal, and optical properties is then combined with the internal characterization to understand the material and find real applications. This field plays a crucial role in various scientific and technological advancements, such as the development of new materials for electronics, energy storage systems, and catalysis[1].

4.1.1 Perovskites

Perovskites are materials with a crystalline structure whose fundamental chemical formula is ABX_3, where A and B are cations of various sizes and X are anions [see figure 1a and figure 1b]. B is a medium-sized cation that prefers octahedral coordination and is typically a transition metal. A is a large cation that can be an alkali, an alkaline earth, or a lanthanide. A perovskite structure is formed by a cubic unit cell containing B site atoms at the centre, X site atoms at the octahedra's edges, and an A site atom at the cell's corner. These ceramics can modify their properties by being doped with different elements, allowing them to modify their crystal structure, alter their conductivity, and make them suitable for use in solar cells.

4.1.2 $BaCo_{0.2}Fe_{0.2}Zr_{0.4}O_{3-\delta}$ (BCFZO)

This work will be talking about the cubic perovskite $BaCo_{0.2}Fe_{0.2}Zr_{0.4}O_{3-\delta}$ which has a unit cell dimension[2] of 4.10175 Å. It is worth noticing that in this case [see Figure 1a and Figure 1d], the A site is a barium atom (green) and the B site can be three different elements: cobalt (dark blue), iron (brown) or zirconium (pink).

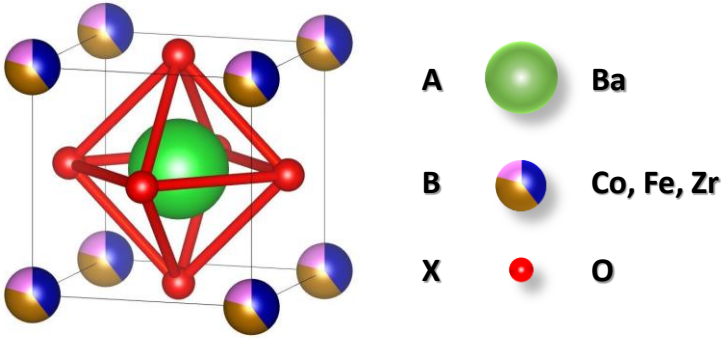

Figure 1: $BaCo_{0.2}Fe_{0.2}Zr_{0.4}O_{3-\delta}$ structure created via VESTA software using the data from literature2. With index corresponding to a general cubic perovskite and color-coded identifiers from both general perovskite and BCFZO structure.

The reference structure was calculated by creating the structure in the visualisation for electronic and structural analysis (VESTA) software and complementing with data, unit cell dimension and space group, from literature[2,3].

This material in particular was chosen because in the latest literature, it is acknowledged to be a long-lasting and high-performing cathode material for protonic ceramic fuel cells[2–4]. An important fact is that all this literature is only centred in powder ceramics experimentation. In other words, the initial aim of this studies is to synthesise the most homogeneous powder possible to make the densest and most homogeneous bars and pellets possible. Through this experimentation these previous studies were trying to determine the bulk properties of the material. These methods, although reliable due to their synthesis processes being historically established and reliable[5,6], always need high synthesis and sintering temperatures (from 1000ºC to 1500ºC)[7] with long dwell time (> 10h) and greater amount of primary materials to produce the samples. Therefore, the aim of this project is to develop a new synthesis methodology to prepare

thin films of the BCFZO material by using a much more environmentally friendly technique: the spin coating[8].

4.2 ELECTRONIC CERAMICS

Electronic ceramics are ceramic materials which have electrical properties, and therefore, specific application. These materials are mostly made of oxide-based materials and widely used in the production of electronic components[1]. They may be divided into five ceramic groups based on their applications and functions: ionic, ferroelectric, semiconductor, insulators, and capacitors[9].

4.2.1 Electric conductor

Taking into account that conductivity refers to a material's ability to transmit electricity or heat, and considering the band theory[5] with both valence and conductivity bands. The electrical conduction can be defined as the movement, or flow, of electrons between these two bands[5]. Electrical conductors [see Figure 2] are those whose valence and conduction bands overlap, allowing electrons to flow within the internal structure, with a very low resistance. An opposite to conductor materials there are insulators. An electrical insulator [see Figure 2] is a material that prevents the free flow of electrical current due to its wide energy gap, that separates the valence from the conduction band. Electrons may always be stimulated into this band at a certain voltage, known as the breakdown voltage [7].

4.2.2 Semiconductor

A semiconductor is a material that, in terms of electrical conductivity, falls between insulators and conductors. So, originally, semiconductors are materials with a crystalline structure, a complete valence band and an intermediate band gap [see Figure 2]. This kind of materials are nowadays interesting due their wide applicability within new technologies[5,7], for example in integrated circuits within any electronic device. By injecting impurities (also known as "doping") into their original crystal structure, their conducting characteristics can be meticulously changed to match the new technological needs. This doping can vary some useful features such as, changeable resistance, the ability to transmit current more freely in one way than another, and sensitivity to heat or light.

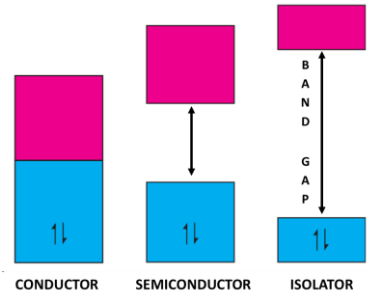

Figure 2: Bands in conductor, semiconductor, and isolator materials[5].

4.2.3 Ionic conductor

As previously seen, an electrical conductor is a material that allows electricity to flow through it, therefore, an ionic conductor is a material that allows small ions, mostly small cations, to move through its internal structure. In most solids, especially crystals, ions rigidly occupy fixed positions, connected to neighbouring ions, creating a defined structure. In some solids, selected ions are highly mobile, allowing ionic conduction, such as Na^+ or Li^+, and more recently, protons, which are of interest due to their applications in new-generation batteries [5].Because of the relative size of ions compared to the holes they are moving in, their mobility and thus their conductivity, in the solid is generally much smaller than the values typically found for electrons [1].

4.2.4 Applications of electronic ceramic materials

Electronic ceramics, capacitors, ferrites, insulators, piezoelectric, and superconductors are critical in the semiconductor industry due to their superior electrical, mechanical, and physical qualities.[7] These ceramics are widely used in the manufacturing of electronic devices. Such as smartphones, computers, televisions, and fuel cells [see Figure 3]. Solid oxide fuel cells (SOFCs), as a type of fuel cell, also help to create a more sustainable energy future. They have higher efficiency and lower emissions compared to traditional combustion-based power generation technologies.

4.3 FUEL CELLS

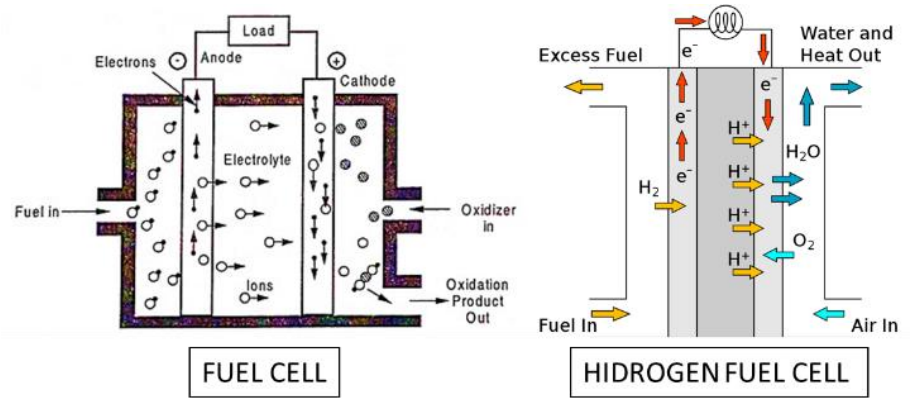

Figure 3: Schematic diagram comparing a fuel cell and a hydrogen fuel cell[10].

Fuel cells are composed of an anode, a cathode, and an electrolyte that allows ions to move between the two sides [see fuel cell in Figure 3]. As a general mechanism of fuel cells, a catalyst at the anode accelerates fuel oxidation, generating ions and electrons[11]. These ions move through the electrolyte, while the electrons move through an external circuit producing electricity. At the cathode, the same or another catalyst, the reduction of other reactants occurs. Fuel cells are classified by electrolyte type and startup time, ranging from 1 second for proton exchange membrane fuel cell (PEMFC) to 10 minutes for solid-oxide fuel cells (SOFCs)[11].

Fuel cells differs from batteries as they require a continuous source of fuel to generate electricity, unlike batteries which rely on existing substances and generate a current. They operate at higher efficiencies than conventional combustion engines, converting chemical energy directly to electrical energy. Fuel cells offer a versatile solution for power generation across various sectors, including transportation, industrial, commercial, and construction[12].

More recently, hydrogen fuel cells [see hydrogen fuel cell in Figure 3] have been emphasized because they use hydrogen and oxygen gas as their main reagents and only emit water vapor as product. For that reason, they have become a target for technological development, addressing climate challenges and reducing air pollutants.

4.3.1 Solid-Oxide Fuel Cells (SOFCs)

Solid oxide fuel cells (SOFCs) are fuel cells composed of ceramic oxides. Considering which is the conducting ion inside the structure, there are two main types of SOFCs: protonic ceramic fuel cells (PCFCs), which use proton-conducting oxides as electrolytes; and traditional oxide ion-conducting fuel cells (O-SOFCs), which use oxygen ion conductors, such as Yttria Stabilised Zirconia (YSZ) [13].

SOFCs are particularly appealing for stationary fuel cells due to their low material cost with non-noble metal catalysts, and high stability due to their all-solid cell configuration. However, a downside of SOFCs is the high working temperatures they need as they usually work at over 800ºC. Therefore, has been an increased interest in PCFCs since they need lower working temperatures[10], around 400ºC, because of the high mobility of protons in the structure. This important fact enables them to provide several valuable benefits, such as prolonged cell lifetimes, and lower operating and selling costs[12]. For example, literature reveals[2,4,14] that BCFZO is a promising cathode material for intermediate temperature PCFCs (300–600 ºC) due to its reduced resistances and enhanced compatibility with advanced electrolytes, such as YSZ.

5. EXPERIMENTAL TECHNIQUES

5.1 SAMPLE SYNTHESIS

5.1.1 Sol-gel

The sol-gel[5] is nowadays a well-known procedure for synthesizing homogeneous multicomponent oxides that consists of 3 steps: hydrolysis, complexation, and polycondensation[15]. Before focusing on the procedures' chemical parameters. It is important to mention that a *sol* is a colloidal suspension of solid particles in a liquid, whereas, a *gel* is made up of a porous, three-dimensionally solid network that surrounds and supports a liquid phase[1,16].Compared to other synthesis techniques, the sol-gel approach has several benefits, such as being able to manipulate the structure and composition and, operating at lower temperatures. Therefore, ceramics, glasses, and other functional materials can be synthesized via sol-gel under moderate conditions[1].

Typically, the reagents for a sol-gel synthesis can be an aqueous solutions of metal salts and a polymeric substance or metal organic compounds that can interact between them[15]. For the first step, hydrolysis, the solvation of the metal salts will be considered. During this step, partial covalent bonds are form, and thus, water molecules become more acidic [see Figure 4Figure 4: Scheme of the solvation procedure of a general metal ion in water.

] due to the partial transfer of an electric charge of a water molecule to the transition metallic ion. This is important in the procedure, because depending on the metal ion, the final pH of the solution might change, and it isa crucial factor during the complexation, which is the next step[1,16].

$$M^{Z+} + nH_2O \rightleftharpoons [M-OH_2]^{Z+} \rightleftharpoons [M-OH]^{(Z-1)+} + H^+ \rightleftharpoons [M=O]^{(Z-2)+} + 2H^+$$

Figure 4: Scheme of the solvation procedure of a general metal ion in water.

Secondly, the complexation takes place when the solvated metals interact between each other and with the polymeric substance, forming metal alkoxides. If the complexation between all

the molecules involved in the reaction is not as predicted, the final structure will vary, and the product won't be the desired one. Hence, the degree of hydrolysis and condensation greatly influences the composition, structure, and viscosity of the reaction products and it must be controlled through the experimentation. Afterwards, the polycondensation is done by drying the initial solution, at around 130 ºC, and it is when the gel structure is formed. This gel is typically used in thin films synthesis by depositing it on a substrate via spin or dip coating. Finally, the gel is then heated, or calcined, to decompose organic matter and leave an oxide product on the selected substrate[5].

5.1.2 Modified Pechini process

The term "modified Pechini process"[17–19] is today mostly used for a process where aqueous solutions are used as precursors in a sol-gel synthetic route. As nowadays organic solvent synthetic routes are an environmental concern, aqueous solutions have become one of the most popular synthetic routes for complex oxide materials due to its simplicity and versatility[17]. The experimental synthetic route followed during the first part of this study was based on the modified Pechini process, in this case two different complexing agents were used to ensure good complexation due to the different metal atoms used.

5.1.3 Polymer-Assisted Deposition (PAD)

On the second part of this project, due to technical difficulties, the process was modified, and the PAD process[20–22] was employed. The most important aspect of PAD is its inherent stability of the product metal polymer solutions. Considering that EDTA [see Figure 5] forms stable complexes with almost all metals and knowing that first row transition metals bind well to polyethyleneimine (PEI)[23,24], a solution with both complexants, it is a stable and well-known working combination[25]. Additionally, during this project, citric acid was also used as a complexant agent.

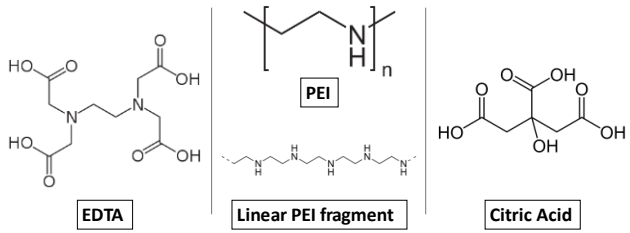

Figure 5: Schematic structures of all three complexant agents used during this study's synthesis.

5.2 SAMPLE PRODUCTION

5.2.1 Spin-coating

Spin coating[8] is a technique used to produce uniform and homogenous thin films on substrates. It involves dropping a small amount of the coating material solution onto the substrate's centre and spinning it at fixed speed (rpm) for a few seconds to disperse it evenly[1,26]. [See each subsection 8.2 for spin conditions depending on the set of samples]

This process can be dynamic or static, with the substrate rotating while the precursor solution is applied or not. Therefore, to ensure uniform layering and prevent layers from interacting with one another, it is necessary to dry, by letting the solvent evaporate, between each layer before adding another[25,27].To prevent the substrate from moving while spinning during the coating process, it must be held by a vacuum system. The most important variables that influence the thickness of the layers are solvent, solution concentration, viscosity, and spinning rate. Even though spin coating is simple, fast, and cost-effective; only one substrate can be used at a time and wastes a significant amount of solution, between 70% and 80%, every time a layer is applied.

5.3 SAMPLE CARACTERISATION

5.3.1 X-ray diffraction

X-ray powder diffraction (XRD) is a characterization technique to identify the phase of crystalline materials and providing information on unit cell dimensions. Monochromatic X-rays from a cathode ray tube are focused into the sample. The incident rays cause constructive interference when the conditions of Bragg's Law [see Formula 1] are met, and by measuring the diffracted beam, it is possible to obtain each possible lattice diffraction orientation of the sample. Converting diffraction peaks to d-spacings facilitates identification through comparison with recognized reference patterns because each crystalline material has a unique diffractogram[5].

$$n \cdot \lambda = 2 \cdot d \cdot \sin(\theta)$$

Formula 1: Bragg's Law[5] where d is the distance (Å) between planes, θ is the angle in degrees of the reflection, and λ is the wavelength of the radiation[6].

All the XRD measurements were performed in Marvel Panalytical-Aeris (Ltd, s.f.). All XRD data was visualized and processed with the FullPorf open software.

It was important to design a program that allowed low noise and detailed measurement, but at the same time, could be done as a relatively fast routine examination. By examining the crystallographic characteristics, we gained a deeper understanding of the film's structural integrity, and potential phase transitions, which are critical factors influencing the material's electrochemical behaviour. Due to these requirements a series three programs were designed. The first one allowed an identification in 5 minutes of primary and secondary crystalline phase, without much detail, divided into two zones: from 2θ=20º to 2θ=23º and from 2θ=29º to 2θ=32º with a 002 step. If the sample had a minimal amount of any of the crystalline phases, a second program from 2θ=20º to 2θ=50º with a 002 step showed the relative amount of each phase in the sample, in 1h. Finally, if the sample had monocrystalline BCFZO phase, a third program from 2θ=10º to 2θ=90º with a 001 step, allowed the samples' exhaustive characterization.

5.3.2 Microscopy

When examining samples with different microscopy techniques, a sequence of steps must be followed, each with higher magnification. The first stage involves bare inspection, reaching submillimetre resolution and a general idea of colour, texture, and macroscopic shape[27]. The second phase involves micron-level observation with an optical microscope and details down to the level of the micron, so that texture and submillimetre shape can be determined. The third stage uses scanning electron microscopy, offering nanoscale resolution and allowing for the examination of surface morphology and fine details at the nanometre level[5].

5.3.2.1 Optical microscopy

Optical microscopes, sometimes referred to as light microscopes, enlarge pictures of small objects using lenses and visible light. Various lighting techniques, such as clear, solid, polarized, or phase-contrast imaging, can be used with optical microscopes[28].To zoom in, objective lenses with multiple magnifications are fixed on a turret with a general maximum magnification power of around 1000 time more[29]. Even with their limited magnification capability, optical microscopes remain indispensable due to their simplicity, affordability, and adaptability. In this study, a reflected light microscope[30] was always used, because what was needed of this characterization technique

was the capability to see the overall texture of the samples and help determine the layers' homogeneity.

5.3.2.2 Electron Microscopy

Figure 6: Picture of the Microscope Leo Gemini 1530-Zeiss

Electron beam interactions with solid targets can be elastic or inelastic. Elastic collisions minimize energy loss and maintain coherent wave properties, resulting in measurable diffraction patterns, like XRD. While inelastic scattering sends most energy to the solid target. In this case the target can react by emitting photons, reemitting secondary electrons, excitation of lattice vibrations, heating the sample, or undergoing radiation damage, which can result in structural alterations[5]. Is through this focused beam of electrons, that scan the sample and reemit secondary electrons after interacting, that scanning electron microscopy (SEM) allows high-resolution imaging and analysis of surface features, such as surface roughness, and in this case study, homogeneity of the thin film[30,31]. It is particularly useful in the study of materials with complex microstructures or nanoscale features. Furthermore, SEM can also be used to determine the elemental composition of a sample through energy-dispersive X-ray spectroscopy (EDS)[5] analysis. For this work the Microscope [see **¡Error! No se encuentra el origen de la referencia.**] Leo Gemini 1530-Zeiss was used to do all the SEM measurements.

5.3.3 Thermogravimetric analysis (TGA)

A TGA is made by tracking a sample's weight while it is heated at a consistent pace in a controlled environment. It is an analytical technique used to determine a material's thermal stability and its proportion of volatile components[32]. After the measurement, not only the different

losses of mass can be compared, but also the difference of energy. Therefore, with this analysis every weight loss can be related to an endothermic or exothermic phenomena in the sample[29].

In this work this technique was used to control the weight loss of the solution during its complete thermal treatment, from solution to oxide powder, and to determine the ideal calcination temperature for calcining all organic component.

5.3.4 Electrical properties and measurements

During this study two main electrical properties have been tested: conductivity and resistance. Electrical conductivity (σ) measures a material's ability to conduct an electrical current, measured in Siemens per meter (S/m). It is important to consider, that conductivity considers the geometry of the sample, while electrical resistance (Ω) measures the general material's resistance [see Formula 2]. This is crucial for experimental measurements, where resistance is measured and then conductivity is calculated.

$$R = V/I$$

Formula 2: Ohm's law, where R is the resistance (Ω), V is the voltage (V), and I the intensity (A) of the current.

$$\sigma = 1/R \times l/S \; ; \quad [S = H \times C]$$

Formula 3: Conductivities' calculation from the resistance, considering the geometrical parameters. Where l is the length and S is the samples' area. S is calculated as the product between the base, C, and the thickness, H, of the samples.

It is important to notice [see Formula 3], that l is the geometrical parameter parallel to the applied current, and thus S is the perpendicular one. In this study, as it was done on thin films, the thickness of the samples was one of the determining factors, but also, one of the most approximated due to experimental complications.

5.3.4.1 2-point vs 4-point electrical measurement

The 4-point probe method is a method used to measure electrical properties using separate pairs of current-carrying and voltage-sensing electrodes. This method is more precise than the conventional two-terminal (2T or 2-point) sensing method and is particularly useful for measuring sheet resistance in thin films. With four points of contact between the sensor and the sample [see

Figure 6], lead and contact resistance are removed from the measurement, allowing for accurate measurement of low resistance values[33].

In this study, in addition to structural characterization, we conducted 2-point and 4-point electrical measurements[7] on some samples to assess the electrical conductivity, and overall electrochemical performance of the BCFZO thin films.

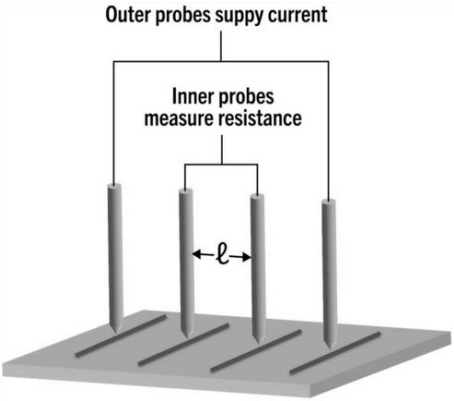

Figure 6: General scheme of a 4-point electrical measurement.

5.3.4.2 Arrhenius equation

Once the resistance and conductivity data are collected, the Arrhenius equation [see Formula 4] can be used to calculate the activation energy (E_a) for the process[13]. First it is important to plot the data and then, the activation energy can be interpreted from the slope of the line.

$$\log(\sigma) = \log(A) + (-Ea/RT)$$

Formula 4: Arrhenius equation where σ is the conductivity in S/m, A is the pre-exponential factor, R is the universal gas constant, T is the temperature in K and Ea is the activation energy in eV.

6. OBJECTIVES

The main objective of this work is to produce $BaCo_{0.4}Fe_{0.4}Zr_{0.2}O_{3-\delta}$ (BCFZO) thin films using a chemical solution-based spin-coating technique for electrical measurements. For accomplishing the main objective, the following specific objectives must be also achieved:

- Detailed control of the precursor calibration and pH parameters during the solution synthesis.
- Optimise the main solutions by maximising their concentration and regulating their viscosity.
- Optimise the deposition process of each layer, minimising production time by adjusting thermal treatments.
- Characterise the thin films on different substrates by X-ray diffraction (XRD) and optical microscopy, ensuring the crystallographic phase and homogeneity of the films.
- Study the electrical properties of BCFZO thin films with most homogeneous surface and crystalline phase.

7. EXPERIMENTAL PROCEDURE

The entire sample production procedure is divided in three different parts: calibration of precursors, synthesis of primary solutions, and production of thin films [See Figure 7]. After, all the samples were characterized by X-ray diffraction pattern (XRD) and optical microscopy, and some of them by SEM.

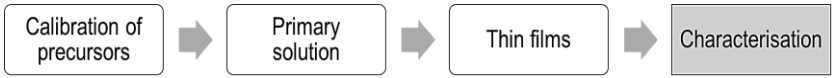

Figure 7: General scheme of the entire experimental procedure

7.1 CALIBRATION OF PRECURSORS

The global objective of this step is to determine the exact amount of metal and water inside a given quantity of each precursor. The four metal hydrated precursors are: iron nitrate ($Fe(NO_3)_2 \cdot 9H_2O$), zirconia nitrate ($ZrO(NO_3)_2 \cdot 4H_2O$), barium nitrate ($Ba(NO_3)_2$), and cobalt nitrate ($Co(NO_3)_3 \cdot 6H_2O$). All bought precursors have an approximate amount of water molecules per molecule of metal. But, because the stoichiometric amount of metal must be perfectly weighted for the compound to form, the exact number of water molecules must be also known.

Table 1: Chemical reactions and temperature during the thermal treatment of different reagents.

Compound	Chemical reaction	Temperature (ºC)
$Fe(NO_3)_2 \cdot 9H_2O$ [34]	$Fe(NO_3)_2 \cdot 9H_2O \rightarrow NO_x \uparrow + H_2O \uparrow + Fe_2O_3$	550 ºC
$ZrO(NO_3)_2 \cdot 4H_2O$ [35 36]	$ZrO(NO_3)_2 \cdot 4H_2O \rightarrow NO_x \uparrow + H_2O \uparrow + ZrO_2$	800 ºC
$Co(NO_3)_3 \cdot 6H_2O$ [37]	$Co(NO_3)_3 \cdot 6H_2O \rightarrow NO_x \uparrow + H_2O \uparrow + Co_3O_4$	800 ºC

To achieve this, an exact amount of hydrated metal nitrate is weighted and decomposed through a thermal treatment to obtain the corresponding metal oxide, excepted for barium [see Table 1]. The difference between the mass of the nitrate and the oxide is then used to calculate the exact amount of water molecules for each precursor.

Barium oxide was calibrated differently because if it had been thermally treated like the rest, the product would be BaO. At room temperature, BaO is unstable and rapidly captures CO_2 to form barium carbonate ($BaCO_3$). Therefore, to prevent its formation, barium nitrate is dehydrated at 110 °C for 4 h and weighted at the same temperature. The temperature of the treatment is chosen according to experimental TGAs in literature [see reference for each precursor in table 1]. All the reagents were treated overnight with a heating/cooling rate of 2.5 °C/h at a concrete temperature. To verify that single phases were indeed obtained after the thermal treatment, a XRD of the resulting powder was performed[38].

7.2 SAMPLE SYNTEHSIS

7.2.1 Synthesis of primary solutions

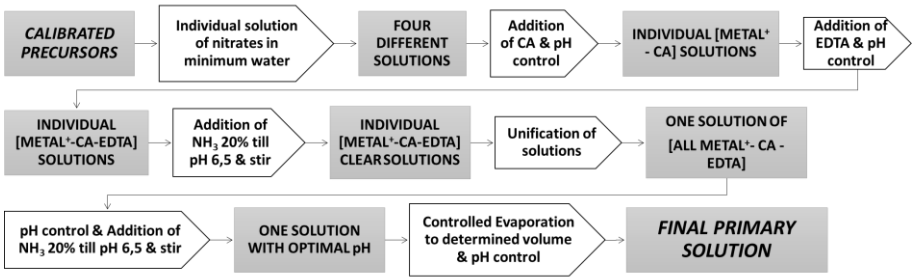

Figure 8: Graphical scheme of the synthesis of primary solutions.

The sample synthesis is performed through a route like the so-called Pechini method[17]. The main difference between the Pechini method and the one performed in this study [see figure 9] is the number of starting solutions. In the Pechini method, all the metals and complexing agents are mixed in one unified solution from the beginning. In this study, to ensure the correct complexation and dilution of every metal nitrate, four different solutions (one for each metal cation) were prepared separately. A 1:1:1 ratio between mol of metal, ethylenediaminetetraacetic acid (EDTA) and citric acid (CA) as complexing agents [see Figure 5], was used to simplify experimentation and because there was literature[2,3,10,19] using this same ratio for Pechini's based experimentation.

During the solution production, the pH was controlled continuously with a pH meter and ammonia addition [see Figure 8]. This is because the optimal working pH for complexing the metal cations with EDTA and CA is between 5 and 6[39,40].

Following the experimental procedure in Figure 9 and having determined a final volume and concentration, the procedure starts by carefully weighting and diluting in the minimum amount of water the nitrate metal salts. This normally resulted in solutions between 10 ml and 20 ml with a pH around 1.7. At this step, iron nitrate and cobalt nitrate solutions resulted in clear solutions, whereas barium and zirconium[41] were whitish dispersions. This is because barium and zirconium have a lower solubility coefficient in water than the other two metals and need the following experimental steps to completely dissolve.

Secondly, citric acid was added. Experimentally, even though it lowered the pH by almost 0.7 in every solution, this helped zirconium nitrate to fully dissolve[42]. Thirdly, EDTA was added, in the doble ammonia salt form. At this point, the pH of all solutions was around 0.8, and the final volume of all solutions was 25 ml approximately. At this point, all the prepared solutions, except the barium solution, were fully clear. Next, pH of all solutions is checked and increased, by the controlled addition of ammonia (NH_3 at 20%), up to pH 6. At this pH it is experimentally observed that the barium solution dissolves immediately and becomes a clear solution.

Figure 9: Picture of the unified solution at pH 6 before evaporating.

Once the four solutions are prepared, they are then unified in a beaker [see Figure 9]. At this point, is important to control the pH because during the additions and mixing of all solutions, it can drop significantly. At this point the pH can get as low as 4, and sometimes a white precipitate can be seen. Considering that all the metal cations were already complexed before they were unified, and due to the abrupt change in pH, it is believed to be EDTA. Also, when the pH is

stabilised again at 6 by adding ammonia, it dissolves completely and a final clear dark red solution of around 300 ml is left [see Figure 9].

The final solution is then heated to evaporate water until the final volume previously determined is reached. At this point, the solution will turn viscous. Finally, the evaporated solution is kept in volumetric flask to ensure the final volume.

7.3 THIN FILM PRODUCTION

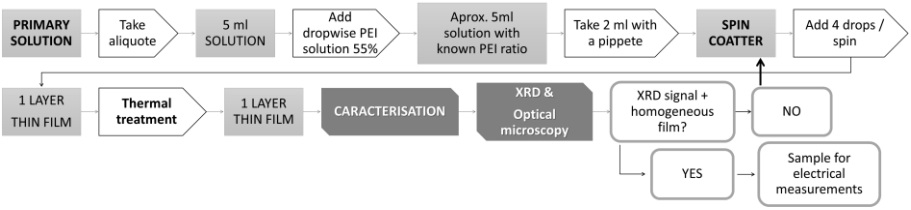

Figure 10: Summarised graphical scheme of the sample production via spin coating.

The optimization of the thin film production is the central part of the study. As it will be later explained on the experimental results (see section 8.2), this study will be focused on PEI[23,24] assisted synthesis. It's important to remember that this solution has the exact concentration of metal cations to finally synthesize the BCFZO crystalline phase. So, the objective of this part will be to prepare thin films of BCFZO deposited on different substrates. This part of the procedure starts by taking al aliquot of the primary solution and adding a known mass of PEI 55% dropwise [see Figure 10]. Repeating this procedure with different PEI mass [calculated with Formula 5], small solutions with different PEI ratio can be made.

$$(\text{mass PEI solution 55\% (g)})/(\text{mol metal in aliquot (mmol)}) = \text{Ratio PEI}$$

Formula 5: PEI ratio's calculation

At this point, a substrate cleaned with ethanol and dried, is put on the spin coater. Every set of samples had optimised spin properties depending on concentration, viscosity, and substrate [see section 8.2]. With the help of a glass pipette, in a dynamic process [see section 5.2.1], 4 drops of the chosen solution are dropped on top of the substrate. Once the spin coater has stopped, the sample is heated on a hot plate at 280 °C. Immediately, the transparent film changes colour into a light brown dried layer. When the sample is already dried, it is treated at higher temperature to promote the formation of the desired product. Different thermal treatments with different conditions were tested during this study [see section 8.2].

Finally, when the thermal treatment is finished, the characterisation begins [see figure 10]. Firstly, the XRD pattern was obtained to confirm the formation of the crystalline phase of the film. Secondly, an optical microscopy observation was performed to verify the homogeneity and check for bubbles and cracks on the film. Finally, if the film was homogeneous and had a pure phase, the electrical performance of the thin film was tested. However, if the XRD characterization revealed the formation of parasitic products or the film was not homogeneous, the sample was again put through the spin coater to add more layers on top and resay [see figure 10].

7.4 POWDER

It was also important during this study to have some reference powder to check and compare the structure with the films, which was achieved by a four-step procedure. Firstly, a primary solutions' aliquot was partially dried on a hot plate at 150 °C. Then, when it started to be thicker, it was transferred to a stove for 24 h at 100 °C. This resulted on a black mass which was put in an oven at 350 °C for 4 h. After this first thermal treatment, black ashes are obtained which were then grounded and put into an alumina crucible. Finally, the last thermal treatment consisting of 8 h at 1050 °C gave the final pure crystalline phase [see Figure 11]. It has been experimentally proved that from 800ºC on, even though not on its most crystalline phase, BCFZO phase is observed.

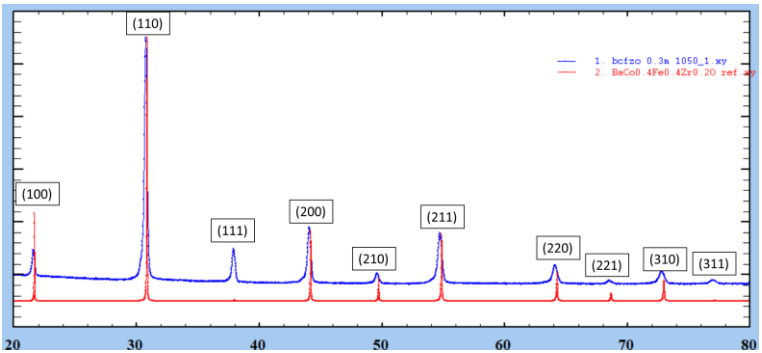

Figure 11: Experimental X-ray diffraction pattern (blue line) of the final reference powder after the 1050ºC for 8h thermal treatment compared to the reference XRD with the planes (red lines) calculated from the VESTA software reference structure. The horizontal axis represents the angle 2θ and the vertical axis represents the normalised intensity of the peaks.

8. RESULTS

8.1 THERMOGRAVIMETRIC ANALYSIS

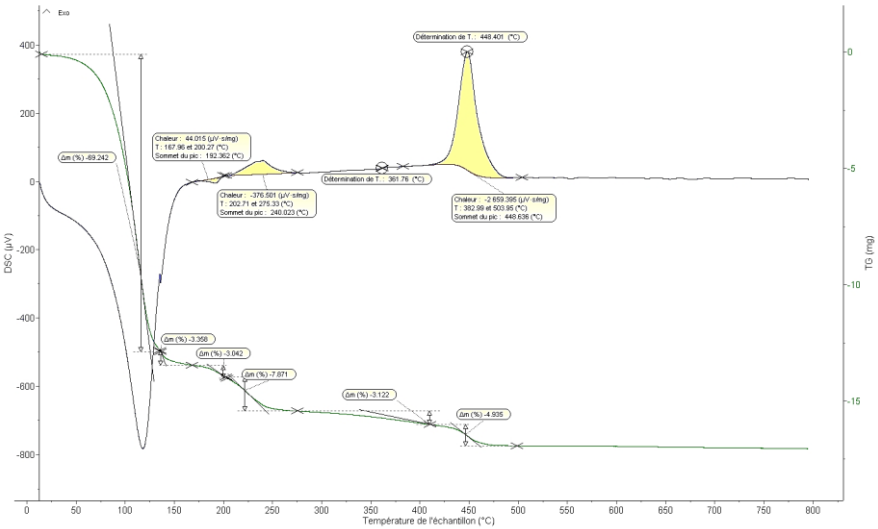

Figure 12: Graph of the thermogravimetric analysis of a drop of a 0.2M primary solution from 0ºC to 800ºC with a 10ºC/hour ramp. Where the blue line is the energy exchange between the sample and its environment, and the green line is the variation of mass with temperature.

In this Thermo-Gravimetric Analysis (TGA), five different events can be differentiated from which three are most relevant concerning our process. From lower to higher temperatures these events are observed at 120 °C, 150 °C, 192 °C, 240 °C, and 448 °C respectively [See Figure 12]. The most characteristic is at 120 ° C with a mass loss of almost 70%, which corresponds to the evaporation of the free water molecules and has the biggest endothermic curve[37] of all the TGA peaks.

The next two small endothermic events appear at 150 ° C and 192 ° C which correspond to the evaporation and decomposition of the nitrate species into different nitrogen species such as NOx gas[34]. The third event, with a maximum at 240 °C is the decomposition of EDTA, CA and other carbon species[26,43] formed during the previous decomposition reactions. Finally, the biggest

exothermic event with a maximum at 450 °C [See Figure 12] is the final decomposition through burning of all carbon containing species[44].

Nevertheless, it is difficult to see a precise a crystallisation temperature from which just BCFZO phase can be detected. From the powder synthesis, it is experimentally known that, at 800 °C, the perovskite phase is already formed, so it could be said that thanks to the high exothermic reaction happening at 450 ºC the first nucleation of the perovskite phase occurs. We could reasonably consider that nanoclusters of the phase are already formed once all carbonaceous species are removed. Considering both TGA results and the observation of a crystalline phase for the powder at 800 °C, we decided to perform the thermal treatments of the thin films above 500 °C.

8.2 THIN FILM SAMPLES

All thin film samples were 12x12x1 mm quartz or glass substrates. They were hand cut with a diamond-tipped tool from a 75x25x1 mm quartz or glass bigger substrates. All thermal treatments of all samples were 3h long with a heating and cooling rate of 95ºC/h.

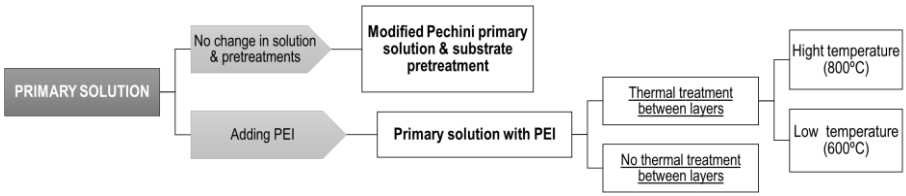

Figure 13: Schematic representation of the different types of samples described in Section 8.2.

As a general picture there were two different typed of samples: with PEI in the solution, and without [see Figure 13]. The samples with PEI in solution gave better results in general, so further experimentation, like different thermal treatment, were done with this samples [see section 8.2.2].

8.2.1 Modified Pechini primary solution & substrate pretreatment

The objective of this samples was to produce thin films out of just the two initial aqueous solutions of 0.2M and 0.3M using two different substates: quartz and glass. The initial hypothesis was that increasing the concentration would increase the viscosity and so, it would produce better films. Also, increasing the concentration would mean decreasing the number of layers needed to have the same results as with a low concentration solution. Regarding the static spin conditions for this set of samples, all of them had a spin time of 30 seconds an acceleration of 3000 s^{-2} and a velocity of 3000 rpm.

At the same time, five different substrate pretreatments were studied on both substrates. All these procedures were done in the aim to interact with the substrate, create a chemical layer on top of the substrate, so later the aqueous solution would interact, lower the wettability between de aqueous solution and the substrate, and improve the thin film formation. Apart from pretreatment (A), the substrates were always rinsed with distilled water and air dried before adding any solution on top. These five different pretreatments consisted of submerging the substrate in different solutions for 10 minutes in:

- Ethanol solution (EtOH 98%) and drying the substrate on the hot plate at 100ºC.
- Ammonia solution (NH_3 20%).
- Nitric acid solution (HNO_3 65%).
- Hydrogen peroxide solution (H_2O_2 30%).
- Hydrogen peroxide solution (H_2O_2 30%), then submerging the substrate in an ammonia solution (NH_3 20%) for 10 more minutes[25,45].
- Hydrogen peroxide solution (H_2O_2 30%), then submerging the substrate in a nitric acid solution (HNO_3 65%for 10 more minutes[25,45].

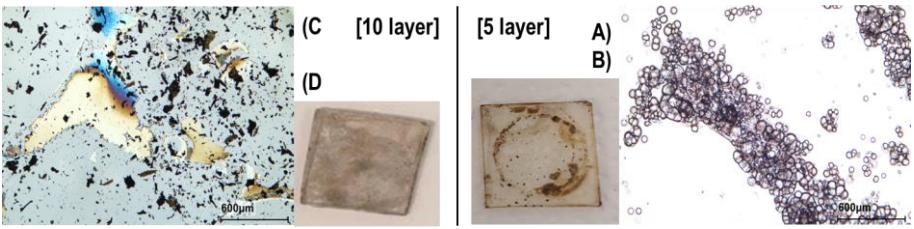

Figure 14: Two representative samples from the set produced from the 0.2M solution using HNO3 65% pretreatment on quartz. Right: A) Optical microscope picture of the 5-layer sample B) Sample with 5 layers. Left: C) Optical microscope picture of the 10-layer sample D) Sample with 10 layers.

Experimentally it was shown that both during the sample production and later during characterisation under the microscope, no homogeneous films were forming on any sample [see Figure 14C and Figure 14B]. Instead, all the material was accumulating in different areas due to a Deweting problem during the spinning process. For example, the grey areas visible on Figure 14D are product, in the form of powder, accumulated and stuck to the quartz.

Also, the XRD patterns didn't show any signal until the films were at least 10 layers [see figure 17]. This can be determined by comparing the spectrum of the 5-layer sample with the spectrum of the bare substrate. In contrast, if we compare it with the 10-layer spectrum [see figure 17], we can see the main peak of the BCFZO at approx. 2θ=30º. The combination of all these characterisation data was what concluded that this procedure did not form thin films on these substrates. Also, that XRD detectors were only able to capture signal when the accumulation of product was in the form of powder and build-up stuck on the substrate was sufficiently high. All these samples were finally discarded, and no electrical measurements were done.

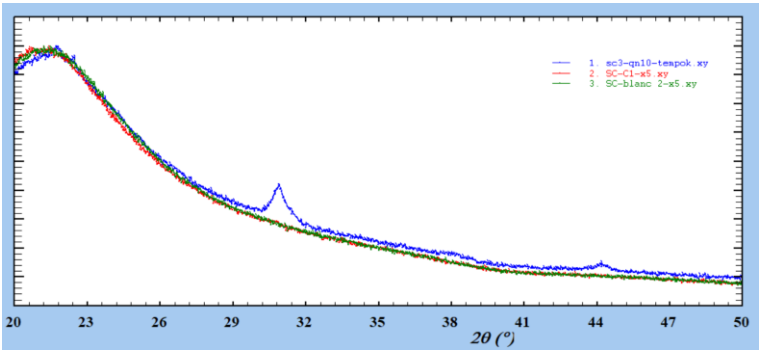

Figure 15: Experimental X-ray diffraction patterns: the 10-layer sample (blue line) from Figure 14, the 5-layer sample (red line) from Figure 16, and the amorphous quartz substrate "blank" (green line). The vertical axis represents the normalised intensity of the peaks.

8.2.2 Primary solution with PEI

The objective of this set of samples was to determine the optimal amount of PEI, or PEI ratio, minimising the change in the concentration of the solution. At the same time, it was important to maintain an optimal viscosity to obtain a homogeneous film on top of the substrates. In terms of experimental characteristics of these samples, just quartz was used as substrate, and six different PEI ratios between 0 and 2,3 were tried [see Figure 16]. Because the results of adding PEI to the solutions were much better than without, more research was done on these solutions. Mainly two types of thermal treatments were carried out: after several layers, or between each layer; besides also comparing thermal treatments at high and low temperature [see Figure 13]. An important experimental observation about this set of samples, is that it was possible to start detecting a crystalline phase by XRD after a minimum number of two deposited layers. Also, spin conditions have been experimentally optimised, and all PEI-containing solutions have a dynamic spin-coating regime.

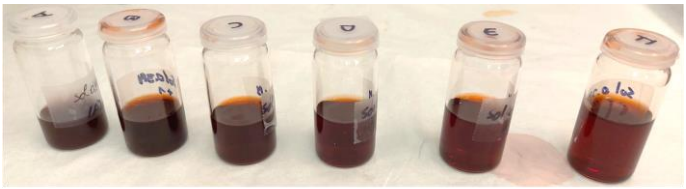

SAMPLE	A	B	C	D	E	F
PEI ratio	0	0.4	0.8	1.2	1.6	2.3

Figure 16: The six different solutions with PEI ratios between 0 and 2.3.

8.2.2.1 Thermal treatment between layers

These samples were at the same time the slowest, and the highest quality samples produced [see Figure 17]. The fact that there was a thermal treatment in between the layers allowed each layer to stabilize and create the thin film before adding another film on top. However, needed almost 24h hours to produce one layer is clearly a disadvantage to the procedure. In this section is important to differentiate between high temperature thermal treatment, 800ºC, and low temperature thermal treatment, 600ºC [See Figure 13]. All these samples were characterised after each deposited layer and had from 2 to 5 layers in total, producing thin films since the first layer. Regarding the spin conditions for this set of samples, all of them had a spin time of 20 seconds, an acceleration of 1000 s^{-2}, and a velocity of 3000 rpm.

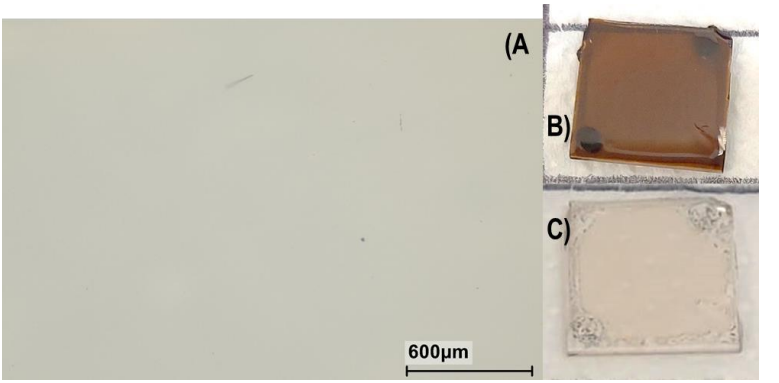

Figure 17: Different pictures of a 2-layer quartz sample from the 0.3M solutions with intermediate hight temperature thermal treatments. A) Optical microscopy picture of a homogeneous thin film. B) Sample after applying second layer and drying on the hot plate. C) Sample after 800ºC thermal treatment.

A general distinguishing feature that can be observed by SEM between [see figure 19] samples that have heat treatments between layers and samples that do not, is the surface roughness. Samples that are not thermally treated have a rougher surface [see Figure 18a], which makes them less homogeneous and, ultimately, their electrical properties are sometimes slightly poorer. However, even if the surface of the samples that do have interlayer treatment is smoother and more homogeneous, due to differences in the expansion index of the material and the substrate, there may be cracks and openings in the films [see Figure 18b].

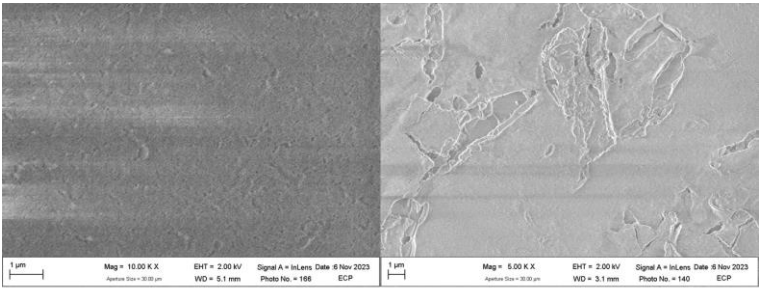

a) No thermal treatment between the 2 layers. **b)** Thermal treatment between the 2 layers.

Figure 18: SEM pictures of 2-layer quartz samples from the set produced from the 0.3M solution at 800ºC thermal treatment.

The high temperature thermal treatment samples usually present a secondary parasite phase [see figure 20], which affected both the XRD patterns and the electrical measurements. All samples tested for electrical properties that had this phase, had much higher resistance that the theoretical expected value. On the other hand, the low temperature thermal treatment samples didn't produce the secondary parasite phase and produced homogeneous films which had better electrical results.

For an overall conclusion, comparing all samples, the best one was the one with a PEI ratio of 1,2 and a lower temperature thermal treatment. This sample was the most homogeneous film, without cracks or build-up, while having an intermediate viscosity during the spin coating. Its electrical results can be seen in section 8.3.

8.2.2.1 Without thermal treatment between layers

These samples gave intermediate results. On one side, it was easier and faster to do the layering than the ones with thermal treatment between layers. On the other side, accumulating more than one layer on top of another one without doing a thermal treatment while working with viscous solutions, was one of the principal reasons for build-up and bubbles in the thin films. In this set of samples, only 800 ºC treatments were done, and so, all samples had both the secondary and the BCFZO phase [See Figure 19]. All these samples were finally discarded because of the poor homogeneity of the films, and no electrical measurements were performed.

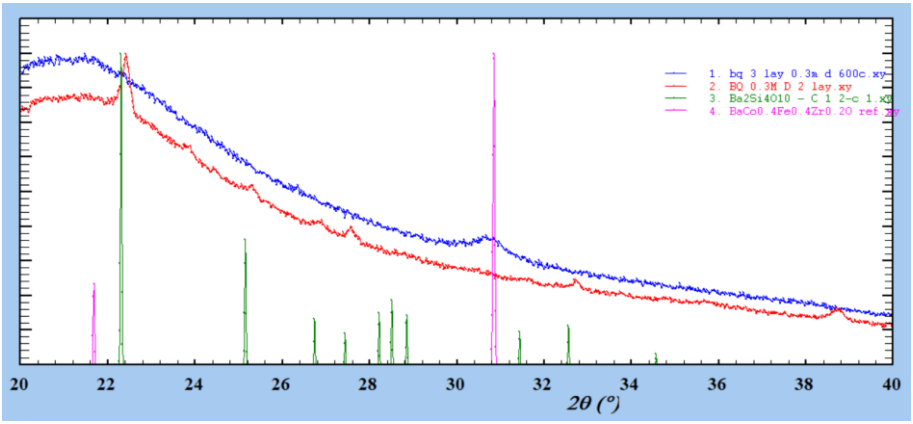

Figure 19: Experimental X-ray diffraction patterns with a 1.2 PEI ratio: 3-layer sample produced form the solution 0.3M at 600ºC (blue line), 2-layer sample produced form the solution 0.3M at 800ºC (red line).

Reference XRD calculated from the VESTA software for structure comparison: BCFZO (pink line), and $Ba_2Si_4O_{10}$ (green line). The vertical axis represents the normalised intensity of the peaks.

Figure 19 is interesting because it can be easily seen how a sample treated at high temperature (red line), not only has a secondary phase (comparing the red line with the most significant peak of the green line), but also has it in a higher relative abundance than the crystalline phase of the BCFZO. However, we can also see in Figure 19 that as soon as the temperature is lowered to 600ºC (now comparing the blue line with the most important peak of the pink line), the samples only show the BCFZO crystalline phase. Regarding the optimised spin conditions for this set of samples, all of them had a spin time of 25 seconds, an acceleration of 1000 s^{-2}, and a velocity of 3000 rpm.

8.2.3 Parasitic phase

At this point, it is important to mention that all substrates used in this study are quartz glass[25] which has a SiO_2 amorphous structure [see Figure 15]. All the samples that have been through a thermal treatment at 800 °C have in common the formation of the same secondary phase [see Figure 19]. Comparing experimental XRD patterns with reference[46] compounds it has been concluded that this parasitic phase is $Ba_2Si_4O_{10}$. This indicates that part of the elements of the compound being synthesised reacts with the substrate during the thermal treatment. If we compare with the phase diagrams of this compound, we can see that it forms at 800 ºC and that once formed, it is stable at room temperature[47]. This fact also implies that this secondary phase increased with every layer and every thermal treatment done at 800ºC[48]. At the same time, on the positive side, in this same study there are experimental data showing that if the thermal treatments are done at a lower temperature than 800°C, this secondary phase does not form [see section 8.2.1 and Figure 19].

8.3 ELECTRICAL MEASUREMENTS

Characterisation of the electrical properties of the thin films was done through a two-step process. Firstly, some electrodes had to be deposited on the films, and this could be done by painting by hand 4 stipes of silver paint on top of the thin film. Once the sample had the electrodes, resistance (Ω) measurements could be performed at different temperatures. An appropriate interface has previously been developed in the LabVIEW software, for programming the Eurotherm, which was used to control the power of the oven and retrieving data from the SR850 on the computer. The resistance measurements were performed from 25ºC to 550ºC in ambient air. Figure 20 shows the base 10 logarithm of the electrical conductivity (log (σ)) as the function of temperature. According to the results, the electrical conductivity of BCFZO oxide gradually rises with increasing temperature. This change in electrical conductivity is not directly analysed but may have its origin in the increase of mobility of the charge carriers (mainly polarons in forms of Fe^{4+} or Co^{4+} on Fe or Co transition metal sites) but can also be affected by the oxygen content inside the material affecting the M^{3+}/M^{4+} ratio. Secondly, once all the experimental data was collected, calculations of conductivity (S/m) and activation energies were done to compare with previous literature[2,4] results. The activation energy of this process is 0.40eV.

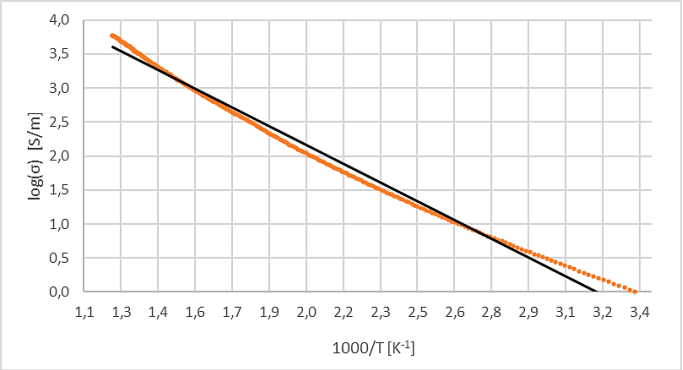

Figure 20: Arrhenius representation of the cooling from 550 ºC to 25ºC

9. CONCLUSIONS

In conclusion, this final degree project was focused on the deposition of $BaCo_{0.4}Fe_{0.4}Zr_{0.2}O_{3-\delta}$ thin films through a chemical solution by spin coating, covering the entire process from precursor calibration to thin film production and characterization, including electrical conductivity analysis [see Figure 7]. The experimental procedure focused on the optimisation of thin film production, particularly PEI-assisted synthesis [see Figure 10]. Despite the different attempts to solve the Deweting issues during the spinning process of non-PEI solutions, the observed buildup of material in multiple places led to the exclusion of samples from electrical measurements, because they were no homogenous film.

Later, the identification of optimal conditions for film production involved thermal treatments on the totality or between layers, distinguishing between high- and low-temperature treatments. The most successful configuration was a PEI ratio of 1.2 with a lower-temperature (600ºC) thermal treatment between layers [see Figure 19], resulting in the production of homogeneous films with acceptable electrical properties. Conducting resistance measurements from 25ºC to 550ºC and combining this data with the Arrhenius equation gave us information about the electrical behaviour of BCFZO. The activation energy for this process was determined to be 0.40 eV [see Figure 20].

Further experimentation recommendations to improve the reproducibility of results should include the crucial need for determining layer thickness for accurate calculations and understanding of thin film electrical properties. Also, further research on samples using a PEI ratio between 1 and 2 and optimising thermal treatments at both temperature (around 600 °C) and time. However, faster sample production with intermediate-fast thermal treatments between each layer at 500 °C could hypothetically result in a more efficient production process and potentially reduce the overall production time and cost. Additionally, on the primary solution side, maintain the solution concentration while exploring variations in the metal: EDTA: CA ratio. As well, alternative polymerization compounds such as ethylene glycol were considered.

10. REFERENCES AND NOTES

(1) Xu, R. Introduction - Frontiers in Modern Inorganic Synthetic Chemistry. In *Modern Inorganic Synthetic Chemistry*; Elsevier, 2011; pp 1–7. https://doi.org/10.1016/B978-0-444-53599-3.10001-0.

(2) Zhang, L.; Shan, J.; Wang, Q. BaCo0.4Fe0.4Zr0.2O3-δ: Evaluation as a Cathode for Ceria-Based Electrolyte IT-SOFCs. *Journal of Alloys and Compounds* **2019**, *771*, 221–227. https://doi.org/10.1016/j.jallcom.2018.08.232.

(3) Qiu, P.; Liu, B.; Wu, L.; Qi, H.; Tu, B.; Li, J.; Jia, L. K-Doped BaCo0.4Fe0.4Zr0.2O3−δ as a Promising Cathode Material for Protonic Ceramic Fuel Cells. *J Adv Ceram* **2022**, *11* (12), 1988–2000. https://doi.org/10.1007/s40145-022-0662-7.

(4) Zohourian, R.; Merkle, R.; Maier, J. Proton Uptake into the Protonic Cathode Material BaCo0.4Fe0.4Zr0.2O3-δ and Comparison to Protonic Electrolyte Materials. *Solid State Ionics* **2017**, *299*, 64–69. https://doi.org/10.1016/j.ssi.2016.09.012.

(5) R. West, A. *Solid State Chemistry and Its Applications*, 2nd ed.; WILEY: UK, 2010; Vol. 83.

(6) Ropp, R. C. *Solid State Chemistry*; Elsevier, 2003.

(7) *Advanced Ceramics for Energy Storage, Thermoelectrics and Photonics*; Elsevier, 2023. https://doi.org/10.1016/C2020-0-03592-9.

(8) Makhlouf, A. S. H. Spin Coating - an Overview. In *Nanocoatings and Ultra-Thin Films*; Elsevier, 2011; pp 3–23. https://doi.org/10.1533/9780857094902.1.3.

(9) Baniya, A.; Pathak, R.; Norris, B.; Li, H.; Rozyyev, V.; Elam, J. W.; Qiao, Q. Next-Generation Battery Technology Based on Solid-State Electrolytes. In *Green Sustainable Process for Chemical and Environmental Engineering and Science*; Elsevier, 2023; pp 1–46. https://doi.org/10.1016/B978-0-323-90635-7.00006-3.

(10) Zohourian, R.; Merkle, R.; Raimondi, G.; Maier, J. Mixed-Conducting Perovskites as Cathode Materials for Protonic Ceramic Fuel Cells: Understanding the Trends in Proton Uptake. *Adv Funct Materials* **2018**, *28* (35), 1801241. https://doi.org/10.1002/adfm.201801241.

(11) Murray-Smith, D. *A Review of Developments in Electrical Battery, Fuel Cell and Energy Recovery Systems for Railway Applications: a Report for the Scottish Association for Public Transport*. https://eprints.gla.ac.uk/204435/ (accessed 2024-01-02).

(12) Cao, J.; Ji, Y.; Shao, Z. Perovskites for Protonic Ceramic Fuel Cells: A Review. *Energy & Environmental Science* **2022**, *15* (6), 2200–2232. https://doi.org/10.1039/D2EE00132B.

(13) Letcher, T. M. Global Warming, Greenhouse Gases, Renewable Energy, and Storing Energy. In *Storing Energy*; Elsevier, 2022; pp 3–12. https://doi.org/10.1016/B978-0-12-824510-1.00011-8.

(14) Raimondi, G.; Longo, A.; Giannici, F.; Merkle, R.; Hoedl, M. F.; Chiara, A.; Sahle, C. J.; Maier, J. Electronic Modifications in (Ba,La)(Fe,Zn,Y)$O_{3-\delta}$ Unveiled by Oxygen K-Edge X-Ray Raman Scattering. *J. Mater. Chem. A* **2022**, *10* (16), 8866–8876. https://doi.org/10.1039/D1TA10211G.

(15) Dislich, H.; Hinz, P. History and Principles of the Sol-Gel Process, and Some New Multicomponent Oxide Coatings. *Journal of Non-Crystalline Solids* **1982**, *48* (1), 11–16. https://doi.org/10.1016/0022-3093(82)90242-3.

(16) Livage, J.; Beteille, F.; Roux, C.; Chatry, M.; Davidson, P. SOL±GEL SYNTHESIS OF OXIDE MATERIALS{.
(17) Sunde, T. O. L.; Grande, T.; Einarsrud, M.-A. Modified Pechini Synthesis of Oxide Powders and Thin Films. In *Handbook of Sol-Gel Science and Technology*; Klein, L., Aparicio, M., Jitianu, A., Eds.; Springer International Publishing: Cham, 2016; pp 1–30. https://doi.org/10.1007/978-3-319-19454-7_130-1.
(18) Pechini, M. P. Method of Preparing Lead and Alkaline Earth Titanates and Niobates and Coating Method Using the Same to Form a Capacitor. US3330697A, July 11, 1967. https://patents.google.com/patent/US3330697A/en (accessed 2023-12-13).
(19) Huízar-Félix, A. M.; Hernández, T.; de la Parra, S.; Ibarra, J.; Kharisov, B. Sol–Gel Based Pechini Method Synthesis and Characterization of Sm1−xCaxFeO3 Perovskite 0.1≤x≤0.5. *Powder Technology* **2012**, *229*, 290–293. https://doi.org/10.1016/j.powtec.2012.06.057.
(20) Ali, M. N.; Garcia, M. A.; Parsons-Moss, T.; Nitsche, H. Polymer-Assisted Deposition of Homogeneous Metal Oxide Films to Produce Nuclear Targets. *Nat Protoc* **2010**, *5* (8), 1440–1446. https://doi.org/10.1038/nprot.2010.105.
(21) Lin, Y.; Gao, M. Polymer-assisted Deposition of Perovskite Dielectric Oxide Thin Films. *IET Nanodielectrics* **2018**, *1* (3), 104–113. https://doi.org/10.1049/iet-nde.2017.0008.
(22) Vila-Fungueiriño, J. M.; Rivas-Murias, B.; Rubio-Zuazo, J.; Carretero-Genevrier, A.; Lazzari, M.; Rivadulla, F. Polymer Assisted Deposition of Epitaxial Oxide Thin Films. *J. Mater. Chem. C* **2018**, *6* (15), 3834–3844. https://doi.org/10.1039/C8TC00626A.
(23) Tang, Z.; Donohoe, S. T.; Robinson, J. M.; Chiarelli, P. A.; Wang, H.-L. Film Formation, Surface Character, and Relative Density for Electrochromic PEI/(PSS:PEDOT) Multilayered Thin Films. *Polymer* **2005**, *46* (21), 9043–9052. https://doi.org/10.1016/j.polymer.2005.07.023.
(24) Kolasińska, M.; Krastev, R.; Warszyński, P. Characteristics of Polyelectrolyte Multilayers: Effect of PEI Anchoring Layer and Posttreatment after Deposition. *Journal of Colloid and Interface Science* **2007**, *305* (1), 46–56. https://doi.org/10.1016/j.jcis.2006.09.035.
(25) *Chemical Solution Deposition of Functional Oxide Thin Films*; Schneller, T., Waser, R., Kosec, M., Payne, D., Eds.; Springer Vienna: Vienna, 2013. https://doi.org/10.1007/978-3-211-99311-8.
(26) Chen, X.; Hu, Y.; Xie, Z.; Wang, H. Chapter 3 - Materials and Design of Photocatalytic Membranes. In *Current Trends and Future Developments on (Bio-) Membranes*; Basile, A., Mozia, S., Molinari, R., Eds.; Elsevier, 2018; pp 71–96. https://doi.org/10.1016/B978-0-12-813549-5.00003-7.
(27) Basile, A.; Ghasemzadeh, K. *Current Trends and Future Developments on (Bio-) Membranes: Microporous Membranes and Membrane Reactors*; Elsevier, 2019.
(28) Zhang, S.; Li, L.; Kumar, A. *Materials Characterization Techniques*; CRC Press, 2008.
(29) Ebnesajjad, S.; Ebnesajjad, C. *Surface Treatment of Materials for Adhesive Bonding*; William Andrew, 2013.
(30) Murphy, D. B.; Davidson, M. W. *Fundamentals of Light Microscopy and Electronic Imaging*; John Wiley & Sons, 2012.
(31) Makowski, G. S. *Advances in Clinical Chemistry*; Elsevier, 2023.
(32) House, J. E. Some Aspects of Dynamic Processes in Solids. In *Dynamic Processes in Solids*; Elsevier, 2023; pp 1–50. https://doi.org/10.1016/B978-0-12-818876-7.00003-9.
(33) *Electrical Measurements, Signal Processing, and Displays*; Webster, J. G., Ed.; Principles and applications in engineering; CRC Press: Boca Raton, Fla., 2004.
(34) Keely, W. M.; Maynor, H. W. Thermal Studies of Nickel, Cobalt, Iron and Copper Oxides and Nitrates. *J. Chem. Eng. Data* **1963**, *8* (3), 297–300. https://doi.org/10.1021/je60018a008.
(35) Liang, J.; Jiang, X.; Liu, G.; Deng, Z.; Zhuang, J.; Li, F.; Li, Y. Characterization and Synthesis of Pure ZrO2 Nanopowders via Sonochemical Method. *Materials Research Bulletin* **2003**, *38* (1), 161–168. https://doi.org/10.1016/S0025-5408(02)01007-3.
(36) Meinel, K.; Eichler, A.; Schindler, K.-M.; Neddermeyer, H. STM, LEED, and DFT Characterization of Epitaxial ZrO2 Films on Pt(111). *Surface Science* **2004**, *562* (1), 204–218. https://doi.org/10.1016/j.susc.2004.06.035.

(37) Ehrhardt, C.; Gjikaj, M.; Brockner, W. Thermal Decomposition of Cobalt Nitrato Compounds: Preparation of Anhydrous Cobalt(II)Nitrate and Its Characterisation by Infrared and Raman Spectra. *Thermochimica Acta* **2005**, *432* (1), 36–40. https://doi.org/10.1016/j.tca.2005.04.010.
(38) Angeles, J.; Matamoros, Z.; Montoya, K.; López-Cuevas, J.; Yanagisawa, K. Synthesis of Perovskite Oxides by Hydrothermal Processing – From Thermodynamic Modelling to Practical Processing Approaches; 2016; p 54. https://doi.org/10.5772/61568.
(39) Danil De Namor, A. F.; Alfredo Pacheco Tanaka, D. Thermodynamics of Protonation and Complexation of EDTA Derivatives and Metal Cations in Water. *Faraday Trans.* **1998**, *94* (20), 3105–3110. https://doi.org/10.1039/a805435e.
(40) Elbagermi, M. A.; Alajtal, A. I.; Edwards, H. G. M.; Azimi, G. H.; Verma, K. D.; Scowen, I. J. RAMAN SPECTROSCOPIC AND POTENTIOMETRIC STUDIES OF ACIDITY LEVEL AND DISSOCIATION OF CITRIC ACID IN AQUEOUS SOLUTION.
(41) Woods, K. N.; Thomas, M. C.; Mitchson, G.; Ditto, J.; Xu, C.; Kayal, D.; Frisella, K. C.; Gustafsson, T.; Garfunkel, E.; Chabal, Y. J.; Johnson, D. C.; Page, C. J. Nonuniform Composition Profiles in Amorphous Multimetal Oxide Thin Films Deposited from Aqueous Solution. *ACS Appl. Mater. Interfaces* **2017**, *9* (42), 37476–37483. https://doi.org/10.1021/acsami.7b12462.
(42) Ekberg, C.; Källvenius, G.; Albinsson, Y.; Brown, P. L. Studies on the Hydrolytic Behavior of Zirconium(IV). *Journal of Solution Chemistry* **2004**, *33* (1), 47–79. https://doi.org/10.1023/B:JOSL.0000026645.41309.d3.
(43) Ludmerczki, R.; Mura, S.; Carbonaro, C. M.; Mandity, I. M.; Carraro, M.; Senes, N.; Garroni, S.; Granozzi, G.; Calvillo, L.; Marras, S.; Malfatti, L.; Innocenzi, P. Carbon Dots from Citric Acid and Its Intermediates Formed by Thermal Decomposition. *Chemistry A European J* **2019**, *25* (51), 11963–11974. https://doi.org/10.1002/chem.201902497.
(44) Chipara, M.; Lozano, K.; Hernandez, A.; Chipara, M. TGA Analysis of Polypropylene–Carbon Nanofibers Composites. *Polymer Degradation and Stability* **2008**, *93* (4), 871–876. https://doi.org/10.1016/j.polymdegradstab.2008.01.001.
(45) Abu Bakar, N.; Mat Salleh, M.; Ali Umar, A.; Shapter, J. G. Direct Deposition of Silver Nanoplates on Quartz Surface by Sequence Pre-Treatment Hydroxylation and Silanisation. *MethodsX* **2017**, *4*, 486–491. https://doi.org/10.1016/j.mex.2017.11.008.
(46) Yao, Y.; Zhou, Z. Photoluminescence Characteristics of a Novel Red Phosphor Ba2Si4O10: Eu3+: Structural Effect and Concentration Quenching Mechanism. *Journal of Luminescence* **2016**, *179*, 408–412. https://doi.org/10.1016/j.jlumin.2016.07.013.
(47) Zhang, R.; Mao, H.; Halli, P.; Taskinen, P. Experimental Phase Stability Investigation of Compounds and Thermodynamic Assessment of the BaO–SiO2 Binary System. *J Mater Sci* **2016**, *51* (10), 4984–4995. https://doi.org/10.1007/s10853-016-9803-0.
(48) Crystal Chemistry of Silica-Rich Barium Silicates: III: Refinement of the Crystal Structures of the Layer Silicates Ba2[Si4O10] (I), (Sanbornite), and Ba2[Si4O10] (h). *Zeitschrift für Kristallographie - Crystalline Materials* **1980**, *153* (1–2), 33–41. https://doi.org/10.1524/zkri.1980.0004.